JOURNAL OF ADVANCED DIELECTRICS
Vol. 8, No. 2 (2018) 1850011 (10 pages)

DOI: 10.1142/S2010135X1850011X

World Scientific
www.worldscientific.com

Manifestation of magnetoelastic interactions in Raman spectra of $Ho_xNd_{1-x}Fe_3(BO_3)_4$ crystals*

A. S. Krylov[†,§], S. N. Sofronova[†], I. A. Gudim[†], S. N. Krylova[†], Rajesh Kumar[‡] and A. N. Vtyurin[†]

[†]*Kirensky Institute of Physics, Federal Research Center KSC SB RAS Krasnoyarsk 660036, Russia*

[‡]*Material Research Laboratory, Discipline of Physics & MEMS Indian Institute of Technology Indore, Simrol 453552, India*

[§]shusy@iph.krasn.ru

Received 24 January 2018; Revised 23 March 2018; Accepted 25 March 2018; Published 24 April 2018

Raman spectra of $Ho_{1-x}Nd_xFe(BO_3)_4$ ($x = 1, 0.75, 0.5, 0.25$) have been studied in temperature range 10–400 K. Two compositions ($x = 1, x = 0.75$) demonstrate structural phase transition with soft mode restoration. The addition of Nd atoms increases interatomic spacing and decreases the temperature of structural phase transition. The solid solutions ($x = 0.75, 0.5, 0.25$) demonstrate the emergence of the peaks corresponding to magnetoelastic interaction below Néel temperature. The order parameter of the magnetic phase transition has been determined. The equal concentrations of holmium and neodymium atoms prevent magnon soft modes condensation caused by exchange interactions in Fe–O–Fe chains are observed. Calculations confirm the data obtained in the experiment.

Keywords: Multiferroic; magnetoelastic interaction; Raman spectra; phase transition; magnetic ordering.

1. Introduction

The crystals of rare earth ferroborates ($ReFe_3(BO_3)_4$, where Re is the rare-earth atom) attract much attention.[1–4] The combination of high physical characteristics and chemical stability of the borates with huntite structure has long been used as elements of optical and optoelectronic devices,[5–7] specifically to add and multiply the laser radiation frequencies.[8,9] Besides, they are observed to have a somewhat unusual structural phase transition between nonpolar phases of trigonal crystal system (from high-temperature $R32$ ($Z = 1$) into low-temperature $P3_121$ ($Z = 3$). The structure with two magnetic ions of different types ($3d$ and $4f$) gives rise to magnetic order at low temperatures.[10] The coexistence of structural and magnetic order parameters can open new opportunities to control their physical characteristics. Despite a significant number of studies on these compounds, some of their properties, in particular, the nature of magnetoelectric polarization, remain unclear. A useful technique for studying these properties is synthesis and investigations of solid solutions with different degrees of substitution of metal and rare-earth ions.

Huntite compounds are characterized by the internal magnetic field (exchange field) induced by the magnetic order established in the samples below the temperature of the magnetic phase transition. This allows us to investigate the feature in the Raman spectra caused by the established magnetic order without external magnetic field.[11] This technique makes it possible to record even minor crystal structure variations and to reveal the character of ion bonds, which can arise from magnetic ordering and magnetoelectric polarization.[12,13]

The features of the huntite vibrational spectrum caused by the magnetic phase transitions have been studied. Adem *et al.*[14] studied Raman spectra of the $TbFe_3(BO_3)_4$ crystal. It was observed that the magnetic phase transition is accompanied by the shift of 200 cm^{-1} and 260 cm^{-1} lines, while the rest of the lines do not significantly move. The authors attributed this effect to the permittivity anomaly at the magnetic phase transition and the permittivity dependence of splitting of the longitudinal and transversal vibration modes.

The structure of high-symmetry phase of these crystals is identical to that cited in Refs. 15–17. It is formed by two helicoidal chains of FeO_6 octahedra with common edges connected by two types of BO_3 plane triangles with rare-earth ions in the cavities between them. It is of interest because the properties of parent compounds — $NdFe_3(BO_3)_4$ and $HoFe_3(BO_3)_4$ — differ quite significantly: $HoFe_3(BO_3)_4$ undergoes a structural phase transition at 360 K, a magnetic phase transition 38.5 K (the easy-plane antiferromagnetic structure AFM2) and a spin-flip phase transition to the easy-

*Selected paper from The International Workshop on Advanced Dielectric Materials and Their Applications, Xi'an, China, Oct. 8–11, 2017.

axis antiferromagnetic structure AFM1 at 5 K. In addition, a spontaneous polarization that can be suppressed by the external magnetic field occurs in the region of existence of the AFM2.[2] On the contrary, the $NdFe_3(BO_3)_4$ crystal remains stable in the structure R32, undergoes a magnetic phase transition at 30.5 K (an easy-plane anti-ferromagnetic structure and exhibits a considerable magnetoelectric effect).[18,19]

The structural phase transition in the holmium ferroborate has not been studied by Raman scattering[20] and is not observed in neodymium ferroborate; at the same time, the ions of these rare earth substantially differ by diameter and this substitution can be expected to bring forth more remarkable effects. The Raman spectroscopy is the appropriate technique for studying these properties which is the synthesis and investigations of solid solutions with different degrees of substitution of metal and rare-earth ions.[21–23] This work continues the investigation of structural and magnetic phase transitions in the rare-earth ferroborates with huntite structure by Raman spectroscopy technique.

2. Experimental

2.1. *Samples*

Single crystal samples were grown from $Bi_2Mo_3O_{12}$-based flux melt[23–25] that reduces replacement of rare-earth ions by bismuth to minimum. X-ray fluorescence analysis (XFA) showed that bismuth content did not exceed 2% in the structure of the synthesized samples. It is convenient to represent the melt-solution system in a quasi-binary form

$$(100-n)\text{wt.\%}[Bi_2Mo_3O_{12}+pB_2O_3+qHo_2O_3 + rNd_2O_3]+n\text{wt.\%}Ho_xNd_{1-x}Fe_3(BO_3)_4.$$

where n is the crystal-forming oxide concentration corresponding to $Ho_xNd_{1-x}Fe_3(BO_3)_4$ stoichiometry and p, q and r are the parameters of the ratio between the crystal-forming oxides in the solution.

The stability regions of the $Ho_xNd_{1-x}Fe_3(BO_3)_4$ crystals and the proportion n and m of the components of the melt solution were determined by the direct phase probing. The saturation temperature was determined with an accuracy of ± 2 K with the use of probe crystals preliminary grown from the same melt solution on a rotating platinum rod under the conditions of spontaneous nucleation. The width $\Delta T_{\text{met}} \approx 12$ K of the metastable phase was found as the maximum overcooling, at which nucleation had not occurred for a period of 20 h.

The melt solutions with different p, q, r and n values were prepared at $T = 1270$–1370 K in a cylindrical platinum crucible by comelting the oxides (Bi_2O_3, MoO_3, B_2O_3, Ho_2O_3, Nd_2O_3, Fe_2O_3) in the proportion given by the above formula. The crucible was placed in a crystallization furnace, where the temperature upward decreased from the crucible bottom with a vertical gradient of 12 K/cm. The melt solution was homogenized at $T = 1323$ K for 24 h. The melt solution was stirred to maintain homogeneity. The saturation temperature determined with the use of probe crystals appeared to be 1238 ± 2 K. First, the crystal with a size of ~ 1 mm was grown in the regime of spontaneous nucleation at the temperature $T = T_{\text{sat}} - (15-20)$ K. The crystal holder with the grown small crystals was taken away without changing the furnace temperature.

Measurements were carried out on oriented crystals sizing $3 \times 2 \times 1.5\ \text{mm}^3$, which did not contain any visible in microscope defects or inclusions.

2.2. *Methods*

The Raman measurements were performed in a backscattering configuration incident light along c-axis of the sample, using a three-grating Raman spectrometer Horiba Jobin Yvon T64000 equipped with a liquid nitrogen-cooled charged coupled device (CCD) detector. The spectral resolution in subtractive mode was better than $2\ \text{cm}^{-1}$ for the frequency region considered. The resolution of low-frequency region when soft mode investigated has been improved to $1.2\ \text{cm}^{-1}$.

The scattering spectrum was excited with Ar^+ laser (wavelength $\lambda = 514$ nm) with 10 mW on the sample; this corresponds to density of laser radiation $30\ \text{W/cm}^2$. The temperature of the phase transition, determined from the spectra, depends on the power of the exciting radiation and shifts to low temperatures with increasing power. This dependence is related to the heating of the sample by a laser beam. Phase transition temperature was found to linearly depend on the power of exciting radiation: $T = (366.33 \pm 0.62)\ \text{K} - (0.41 \pm 0.03)\ \text{K/mW} \times P\ \text{mW}$ for $HoFe_3(BO_3)_4$ (Fig. 1(a)) and $T = (202.9 \pm 1.8)\ \text{K} - (0.8 \pm 0.1)\ \text{K/mW} \times P\ \text{mW}$ for $Ho_{0.75}Nd_{0.25}Fe_3(BO_3)_4$ (Fig. 1(b)), respectively. Temperature variation connected with sample heating by power-stabilized exciting laser radiation was considered constant. All temperature measurements were corrected to the zero exciting power.

The compounds see an identical magnetic propagation vector τ = [0,0,1/2] within the $P3_121$ crystallographic space group which appears at Néel temperature of $T_N = 38$ K for the $HoFe_3(BO_3)_4$ compound. The strong polarization effect of the Fe sublattice on the Ho^{3+} ions leads to simultaneous ordering of both sublattices while the competition between their anisotropies governs the spin-reorientation process at $T_{\text{SR}} = 5$ K.[2] For the $NdFe_3(BO_3)_4$ compound, the Néel temperature of $T_N = 38$ K was determined.[26]

Interaction of structural and magnetic order parameters seems to affect crystal lattice dynamics; this can be observed in its vibration spectrum. Given this in this work, we studied Raman spectra in the vicinity of structural and magnetic phase transitions in $HoFe_3(BO_3)_4$ crystal and in (Ho–Nd) $Fe_3(BO_3)_4$ solid solutions.

The low-temperature experiments were carried out using a closed cycle helium cryostat ARS CS204-X1.SS, controlled by LakeShore 340 temperature controller. The temperature

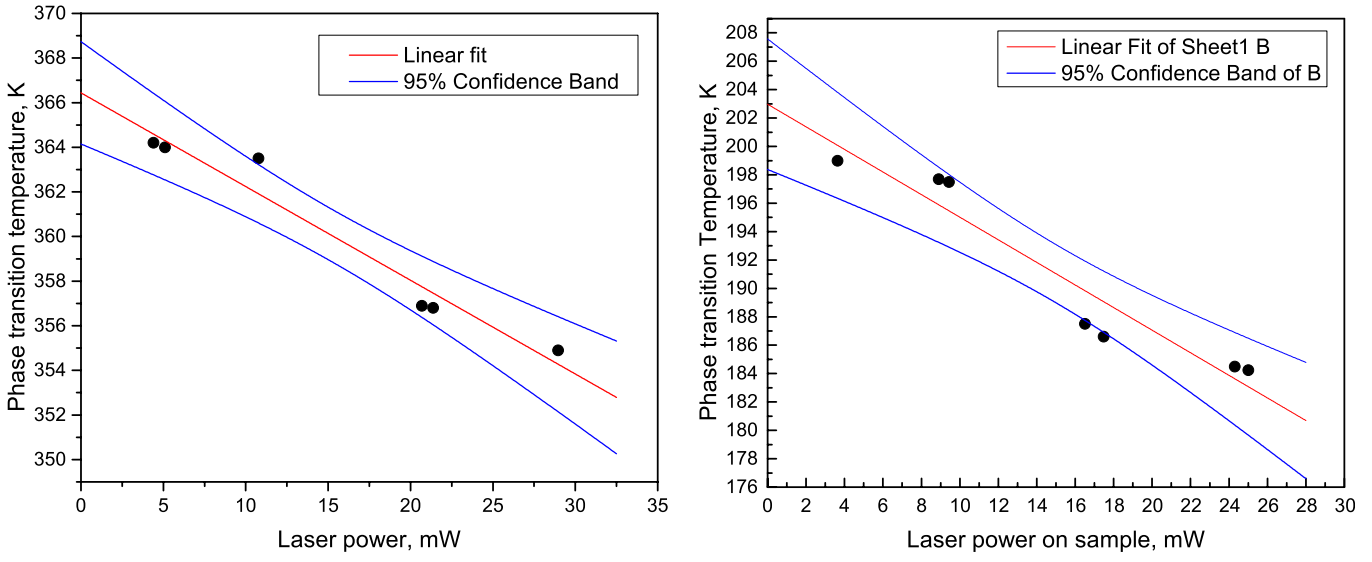

Fig. 1. Phase transition temperature versus pumping power. The lines correspond to linear approximation and confidence range for (a) $HoFe_3(BO_3)_4$ and (b) $Ho_{0.75}Nd_{0.25}Fe_3(BO_3)_4$.

was monitored by a calibrated silicon diode LakeShore DT-670SD1.4L. Indium foil was used as a thermal interface. Measurements were taken inside the cryostat under pressure of 10^{-6} mBar. An Ar^+ ion laser with $\lambda = 514.5$ nm and power 7 mW on a sample was used as an excitation light source. The above instrumentation allows varying the sample cooling rate from 0.1 K/min up to 0.7 K/min with 0.1 K/min intervals.

The experiments were carried out in the dynamic regime by varying the sample temperature and it was identical to the measurement procedure at our past work.[27] The rates of temperature variation ranged from 0.1 K/min to 0.3 K/min in different experiments. The uncertainty of the measured temperature for a given rate can be estimated as a difference between adjacent measurements. Overall time for taking a single spectrum was within 30 s. The spectra were acquired with a temperature step from 0.1 K to 0.25 K.

Quantitative analysis of temperature dependencies in the low-frequency spectrum was carried out with damped harmonic oscillator function (DHO — damped harmonic oscillator).

$$I(\omega) = \frac{1}{F(\omega, T)} \cdot \sum_i \frac{2A_i\omega_{0i}^2\gamma_i\omega}{(\omega_{0i}^2 - \omega^2)^2 + 4\gamma_i^2\omega^2}, \quad (1)$$

where $A, \omega_0, \omega, \gamma$ are the intensity, harmonic wavenumber and damping constant, respectively. Temperature factor $A, \omega_0, \omega, \gamma$ is calculated by formulas

$$F(\omega, T) = \begin{cases} n(\omega) + 1, & \text{Stokes}, \\ n(\omega), & \text{anti-Stokes}, \end{cases} \quad (2)$$

$$n(\omega) = \left[\exp\left(\frac{\hbar\omega}{k_B T}\right) - 1\right]^{-1}. \quad (3)$$

Here, $\hbar$ and k_B are the Plank constant and Boltzmann constant, respectively.

2.3. *Group-theoretical analysis of high-temperature structure R32*

The high-temperature structure of $HoFe_3(BO_3)_4$ contains 20 atoms in a primitive cell and, as result of that, 60 normal modes, 3 acoustical and 57 optical modes. We perform the factor-group analysis to find the symmetries of modes using the local symmetry of all the atomic positions.[28,29] After subtraction of acoustic modes, the optical vibrational modes of the crystal according to results of other work,[15,20] are as follows:

$$\Gamma_{\text{vibr}} = 7A_1(xx, yy, zz) + 12A_2 + 19E(xy, xz, yz). \quad (4)$$

Notations in parentheses refer to the polarizability tensor Raman activity. The modes A_1 is Raman active and A_2 IR active. Doubly degenerated E modes are polar and both IR and Raman active. The light propagating along the c-axis ($\mathbf{k} \| c$) probes transverse optical phonon mode (TO), while the ($\mathbf{k} \perp c$) configuration gives pure longitudinal optical phonon mode (LO).[15]

2.4. *Group-theoretical analysis of low-temperature structure $P3_121$*

The primitive cell of the low-temperature structure contains three formula units — there are 60 atoms,[20] and consequence gives 180 modes, 3 acoustical and 177 optical modes. Performing the low-temperature phase $P3_121$ factor-group analysis, we found the following vibrational modes:

$$\Gamma_{\text{vibr}} = 27A_1 + 32A_2 + 59E. \quad (5)$$

The Raman spectrum includes A_1 and E modes whereas IR includes A_2 and E modes.

2.5. *Computational details*

Within model — rigid ion model[30] — a crystal is considered to consists of isolated spherical ions with ionic charges Z_i, and the potential function is presented as a sum of non-Coulomb and electrostatic contributions:

$$U^{\mathrm{RIM}} = U + \frac{1}{2}\sum_{i,j}\frac{Z_i Z_j}{r_{ij}}. \tag{6}$$

Within this model, only pairwise interactions are considered. They are described by any analytical function $\phi(|R_{ij}|)$ of inter-atomic distance $r_{ij} = x_i - x_j$. The corresponding potential function is expressed as $U = \sum_{i<j}\phi(r_{ij})$. The corresponding contributions to all the quantities can be easily expressed through two parameters $\phi'' = A$ and $B = \phi'/r$ (so-called longitudinal and transversal force constants) and presented in Table 1. The second energy derivative is

$$V_{ij} = U_{ij} + Z_i C_{ij} Z_j, \tag{7}$$

where

$$C_{ij}^{\alpha\beta} = \frac{Z_i Z_j}{r_{ij}^3}\left(3\frac{r_{ij}^{\alpha} r_{ij}^{\beta}}{r_{ij}^2} - \delta_{\alpha\beta}\right), \tag{8}$$

$$U_{ij}^{\alpha\beta} = (A - B)\frac{r_{ij}^{\alpha} r_{ij}^{\beta}}{r_{ij}^2} - \delta_{\alpha\beta} B. \tag{9}$$

The electrostatic contribution calculates the Ewald method. U_{ij} calculates in frame Born–Karman model. Two Born–Karman model parameters are different for a different pair of ions.

Lattice vibration calculation consists of evaluation and diagonalization of the dynamic matrix:

$$D_{ij}^{\alpha\beta} = \frac{1}{\sqrt{m_i m_j}} V_{ij}^{\alpha\beta} \sum_j D_{ij} h_{jn} = \lambda_n h_{jn}. \tag{10}$$

Table 1. Force constant.

Ion	Ion	$A(10^{-18}\,\mathrm{J/A^2})$	$B(10^{-18}\,\mathrm{J/A^2})$	
Nd	B	300.17	0.39	
Nd	Fe	250.17	0.38	
Nd	O	310.17	0.34	
B	Fe	350.17	0.35	
B	O	350.17	0.268	for $NdFe_3(BO_3)_4$
Fe	Fe	250.17	0.383	
Fe	O	336.17	0.365	for $NdFe_3(BO_3)_4$
O	O	306.17	0.389	
B	B	250.17	0.34	
Ho	B	300.17	0.39	
Ho	Fe	250.17	0.38	
Ho	O	310.17	0.333	
B	O	350.17	0.269	for $HoFe_3(BO_3)_4$
Fe	O	336.17	0.364	for $HoFe_3(BO_3)_4$

Table 2. Experimental ($T = 293\,\mathrm{K}$) and calculated modes of $NdFe_3(BO_3)_4$.

A		E		
Experiment	Calculation	Calculation	Experiment	Experiment
180	167	113	89 (TO)	93 (LO)
298	311	156		159 (LO)
473	468	202		193 (LO)
636	647	219		232 (LO)
950	953	249	260 (TO)	266 (LO)
1220	1235	268	272 (TO)	281 (LO)
		297	312 (TO)	332 (LO)
		341		356 (LO)
		358	354 (TO)	384 (LO)
				439 (LO)
		446	475 (TO)	488 (LO)
		562	579	
		641	625	
		660		
		691	669	
		717	734	
		963	968	
			1195	
		1232	1218	
		1252	1244	
		1285	1260	
			1413	

Vibration frequencies calculated for $NdFe_3(BO_3)_4$ and $HoFe_3(BO_3)_4$ crystals are given in the tables together with the experimental values. Calculation for $NdFe_3(BO_3)_4$ crystal was carried out in $R32$ structure, the coordinates of atoms are taken from the neutronography data,[19] experimental vibration data are taken from Ref. 20. Table 2 represents the comparison of the calculated and experimental results.

For $HoFe_3(BO_3)_4$ crystal, the calculation was done for both high-temperature ($R32$) and low-temperature ($P3_121$) phases and is presented in Table 3, Atomic coordinates are also taken from the neutronography data[2] for 520 K in the high-temperature phase and 295 K in the low-temperature phase. Our calculus does not allow taking into account the splitting of longitudinal and transverse vibrations; however, from the tables, it is apparent that calculation results qualitatively agree with the experimental data. Theoretical vibration spectra of $NdFe_3(BO_3)_4$ and $HoFe_3(BO_3)_4$ crystals in $R32$ structure differ little from each other; this is in good agreement with the experimental data presented in Ref. 20. As a consequence, considerable changes in the solid solution spectra can hardly be expected either. Structural phase transition goes without altering the crystal class with the tripling of the cell, the local symmetry of BO_3, FeO_6, ReO_6 decreases; however, as these groups are localized, and distant from each other, internal vibrations of these groups do not undergo considerable changes — near-frequency vibrations emerge.[24,31,32]

Table 3. Experimental ($T = 293$ K) and calculated vibrational modes of $HoFe_3(BO_3)_4$ crystal.

Calculation, cm^{-1}	Calculation, cm^{-1}	Symmetry type	Experiment, cm^{-1}	Calculation, cm^{-1}	Calculation, cm^{-1}	Symmetry type	Experiment, cm^{-1}
Phase $R32$	Phase $P3_121$			Phase $R32$	Phase $P3_121$		
	95	A_1	44	471	463	A_1	470
	99	E	48		471	E	
109	113	E	86		486	A_1	
	122	E	90		499	E	
	137	A_1	92		514	A_1	489
161	163	E	94		541	E	578
			146				592
			158				618
			168				
172	173	A_1	182	567	565	E	
	179	A_1			569	A_1	
	182	E			571	E	
	185	E			586	E	
	187	E			631	A_1	632
	191	E			642	E	673
	193	E	186	650	648	A_1	678
	195	A_1	189	646	649	E	733
	206	E	201		654	E	
211	212	E	207	669	672	E	
	214	E	230		685	E	
223	226	E	249	702	698	E	
	239	A_1	274		721	E	
	245	E	278	727	727	E	
250	247	E	283		737	E	
	254	E			743	A_1	
	263	A_1			747	E	
	264	E			753	A_1	
269	267	E		953	948	A_1	
	269	A_1			950	E	
	278	E		960	960	E	
	289	E			973	A_1	968
300	299	E			974	E	
	309	A_1	308	985	990	A_1	993
	312	E	313		1003	E	1205
	315	E	316		1167	E	1223
318	315	A_1	323		1169	A_1	
	328	E	327		1170	E	
	337	A_1	331	1237	1243	E	
	338	E	346	1240	1244	A_1	1226
346	344	E	350		1249	E	1245
	351	E	360		1263	A_1	1256
			369				1287
	356	E	372	1261	1265	E	1334
367	370	E	397	1288	1309	E	1405
	375	E	400		1331	E	1415
	377	A_1	447		1332	A_1	1451
448	457	E	460		1334	E	1483
							1494

3. Results and Discussion

The spectra of $Ho_xNd_{1-x}Fe(BO_3)_4$ for $x = 1, 0.75, 0.50, 0.25$ measured at 10 K are presented in Fig. 2. Two compositions: $HoFe(BO_3)_4$ and $Ho_{0.75}Nd_{0.25}Fe(BO_3)_4$ at 10 K are in the low-temperature phase with $P3_121$ symmetry, compositions: $Ho_{0.5}Nd_{0.5}Fe(BO_3)_4$ and $Ho_{0.25}Nd_{0.75}Fe(BO_3)_4$ are in the phase with $R32$ symmetry.

Figure 2 shows the general view of the spectrum in the low-temperature phase for all crystals under study and is completely analogous to the spectra of other ferroborates; its detailed analysis is given in Ref. 25. With temperature decrease, two crystals exhibit structural phase transition manifesting in the emergence of several new lines in compliance with changes in the lattice symmetry. In $HoFe_3(BO_3)_4$, the transition is observed at 366 K, which is somewhat lower than $T_{ec} = 420$ K, observed by the authors [Ref. 9 from PR] and is associated with different methods of synthesis; in $(Ho–Nd)Fe_3(BO_3)_4$, the transition shifts towards 200 K. In analogy with the crystals of other rare-earth ferroborates, the soft phonon mode is observed to restore below the structural transition (Figs. 3 and 4); however, temperature hysteresis phenomena are not observed in the solid solution (or the hysteresis value does not exceed 0.1 K), and the soft mode condensation is accompanied by considerable increase of damping — the latter seems to be connected with a large number of structural defects.

The investigation of $Nd_xHo_{1-x}Fe_3(BO_3)_4$ solid solutions for concentrations $x = 0.25$, 0.5 and 0.75 showed that with temperature decrease below the Néel temperature, one of the vibrational modes in the range of 600–650 cm^{-1} increases its intensity (Fig. 5). In this spectral region below Néel temperature, two vibrational modes are observed. One of them persists in spectra in all temperature range. The second one emerges below magnetic ordering transition. The ratio

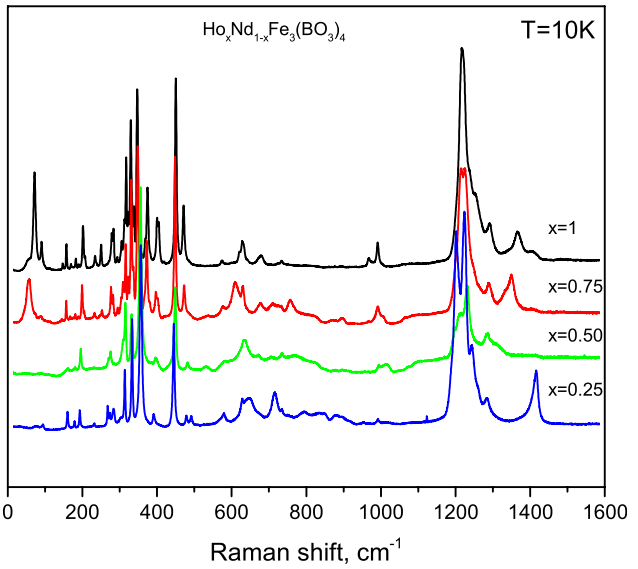

Fig. 2. Spectra of all studied crystals at temperature 10 K.

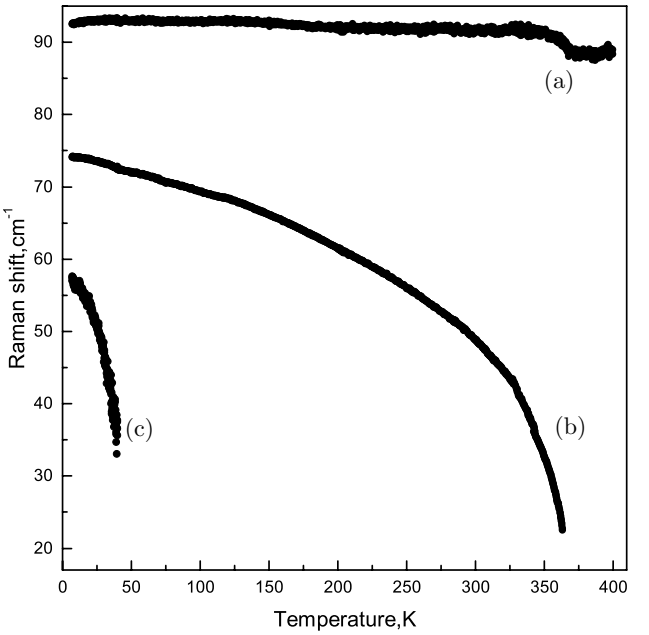

Fig. 3. Behavior of $HoFe_3(BO_3)_4$ modes: (a) hard mode (b) structural soft mode and (c) two-magnon scattering soft mode.

between integral peak intensities describes the order parameter of the magnetic phase transition. Line approximation of the behavior gives Néel temperature point. The two-magnon scattering in compounds of this kind is observed in the frequency range from 60 cm^{-1} to 100 cm^{-1} and there is no reason to believe that in a solid solution, the frequency of the two-magnon scattering is so high — this value is determined by exchange interaction in Fe chains (Fig. 6). The most probable cause of the emergence of this peak is the magnetoelastic interactions. Experimental and theoretical data[20] formed the basis to suggest that below T_N, the symmetry of the crystal decreases due to magnetoelastic coupling with the magnetic moment; this should give rise to new vibration modes in the spectrum. However, experiments on Raman scattering[20] in pure $ReFe_3(BO_3)_4$ (Re = Y, Nd, Pr) compounds did not show this effect; the structural changes may probably be too small for the sensitivity of Raman spectroscopy to record it. In our case, these structural changes are somewhat bigger than in pure compounds because the solid solution is formed by rare-earth elements with substantially different ion radii (Nd — 0.983 Å, Ho — 0.90 Å). Practically, all solid solutions except $x = 0.5$ demonstrate two-magnon scattering features in the low-frequency region. Condensation of two-magnon scattering modes with temperature is presented in Fig. 7. We can determine the temperature of two-magnon mode appearing by the critical behavior: $x = 1$, $T = 38$ K; $x = 0.75$ $T = 34$; $x = 0.25$, $T = 22$ K.

The primary feature of the iron spin ordering is the arising of a broad structured scattering band around 60 cm^{-1} ascribed to two-magnon Raman scattering involving the creation of a pair of magnons with wave vectors $\mathbf{k}$ and $-\mathbf{k}$. Below the Néel temperature, temperature evolution of this broad

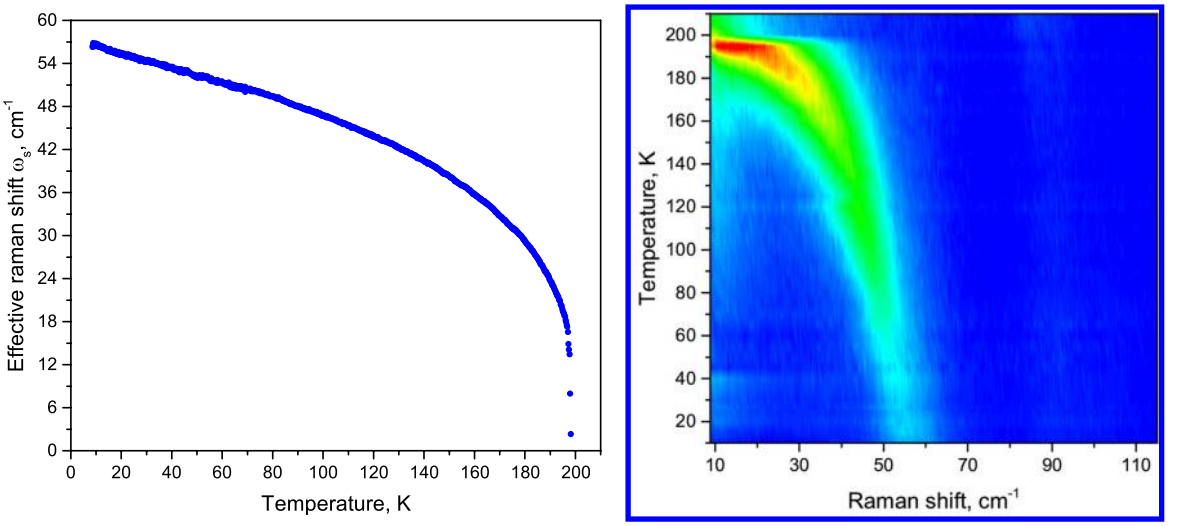

Fig. 4. Structural soft mode in $Ho_{0.75}Nd_{0.25}Fe_3(BO_3)_4$: (a) line position (b) and Raman intensity map.

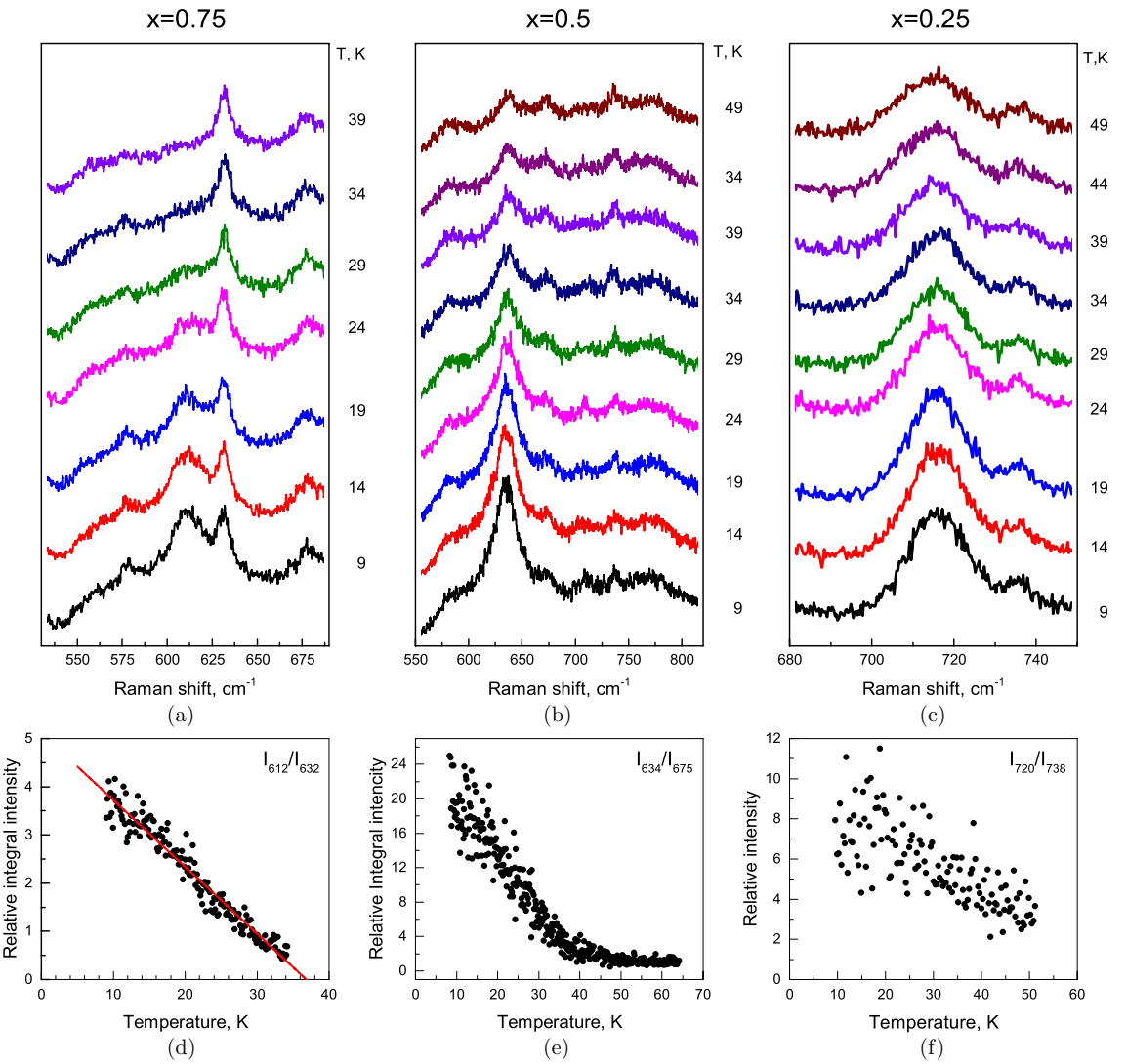

Fig. 5. Relative Raman signal versus temperature.

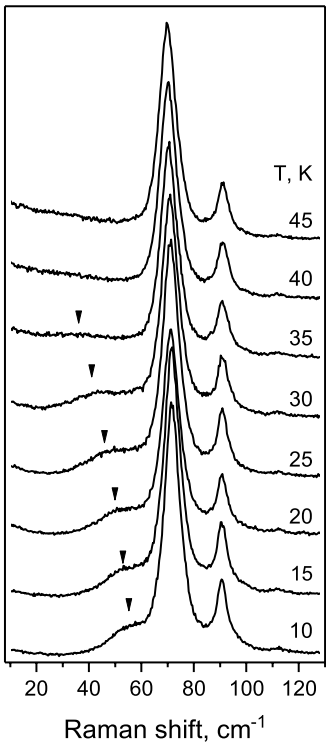

Fig. 6. Transformation of spectra of $HoFe_3(BO_3)_4$ magnon. The arrow indicates two-magnon scattering.

magnetic scattering signature shows this characteristic feature for all the different investigated solid solutions. The most efficient mechanism of two-magnon scattering in antiferromagnets is usually the exchange-scattering mechanism, and the strongest exchange interaction is between the iron atoms along the helicoidal chains, these peaks presumably arise from three magnon branches representing spin excitations on the iron chains.

Relatively small amount of Nd reasonably increases lattice parameters for O and B ions surrounded by Ho to have more freedom. Magnetoelastic interactions in a higher degree affect the shifts of oxygen ions immediately associated with iron ions.

The shifts of oxygen ions are determined by lattice parameters calculation in the low-symmetry phase based on experimental values of vibrations frequencies of $HoFe_3(BO_3)_4$ crystal. Then, similar calculation was made with lattice parameters for solid solutions for different values of coordinates of oxygen ions; we monitored, at this, how the intensity of different vibration modes varies.

Differences in the composition and symmetry notwithstanding, the spectra of all four compounds are very similar. Earlier studies of Raman spectra of the whole range of rare-earth ferroborates showed that the rare-earth ion affects the spectra insignificantly, most lines shift by 5–10 cm^{-1}, and only individual lines shift by 10%, mostly in the low-frequency range where the contribution of a rare-earth element is remarkable. This is because the vibration spectrum of rare-earth ferroborate to a considerable extent is formed by internal vibrations of BO_3, FeO_6 and ReO_6 groups. Structural phase transition does not bring forth considerable changes in the spectra either. Tripling of the cell notwithstanding, significant movement on the frequencies is not observed, the lines split, but because of considerable localization of modes of BO_3, FeO_6 and ReO_6 groups, this does not cause cardinal changes in the spectrum.

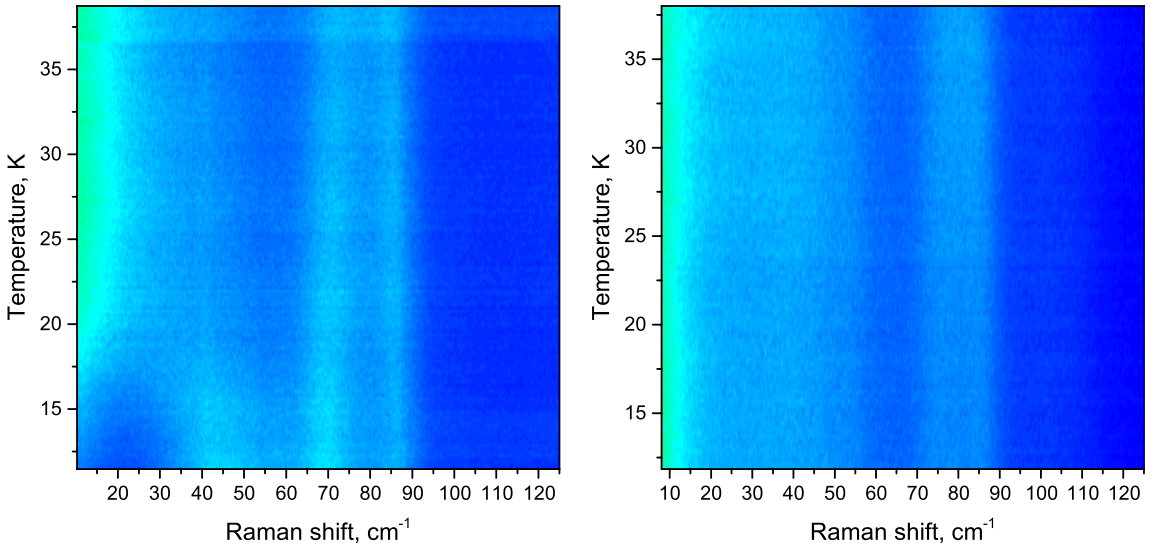

Fig. 7. Behavior of line in the range of two-magnon scattering in $Ho_xNd_{1-x}Fe(BO_3)_4$: (a) $x = 0.25$, (b) $x = 0.50$, (c) $x = 0.75$, and (d) $x = 1$. Only $x = 0.75$ and $x = 1$ demonstrate the structural phase transition and accompanying soft mode. The most intensive lines are phonon lines, two-magnon scattering lowest wavenumber lines.

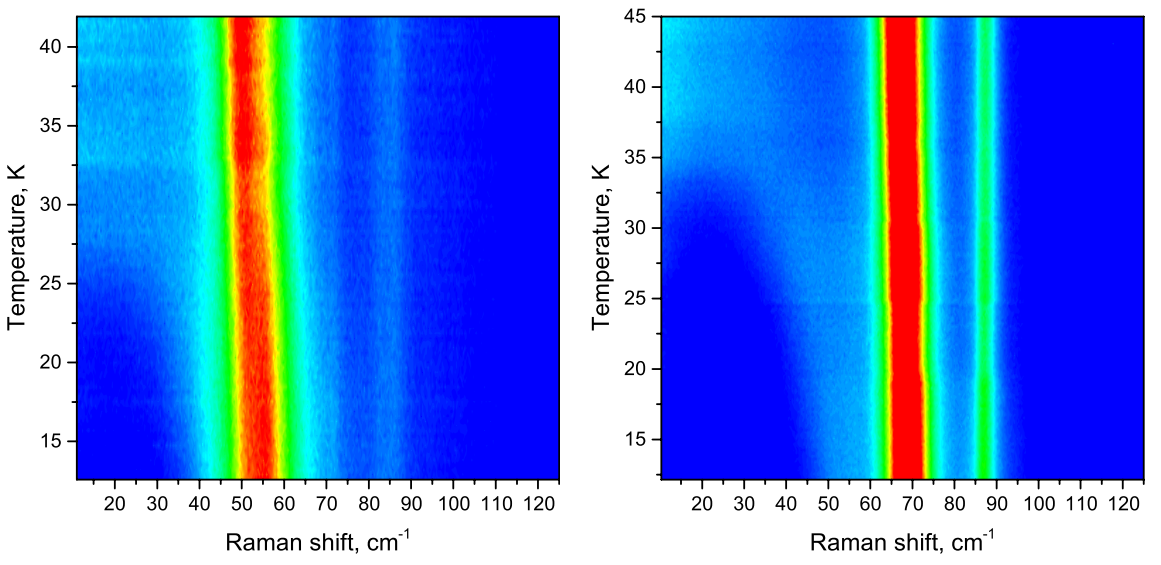

Fig. 7. (*Continued*)

All measured critical phenomena temperatures of all investigated solid solutions $Ho_xNd_{1-x}Fe(BO_3)_4$ are presented in complex phase diagram Composition–Temperature (Fig. 8). The temperatures of the structural phase transition are denoted by black dots and phase boundary approximated by the red curve. The temperatures of the magnetic ordering transition corresponding to Néel temperature are denoted by blue stars and boundary approximated by the blue curve. The crossing of the boundary curves gives us the composition ($0.51 < x < 0.6$) of the coexistence of the structural and magnetic ordering transitions at the same temperature (about 42 K).

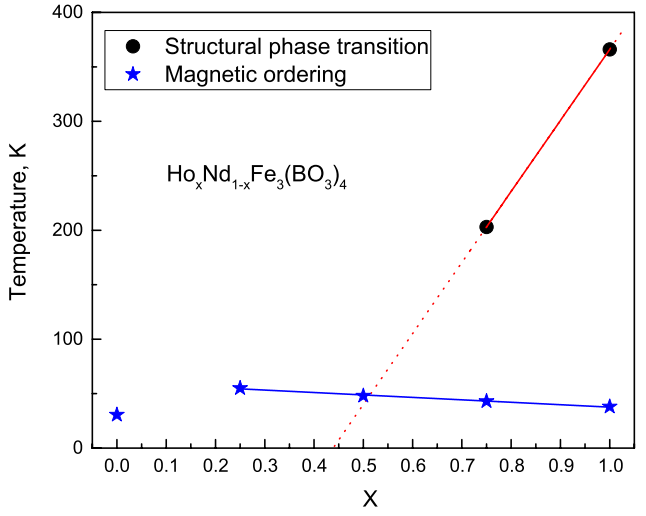

Fig. 8. The phase diagram Composition–Temperature.

4. Conclusion

In the present work, we report the results of Raman scattering investigation and numerical calculation of the structural changes in the solid solutions of rare-earth ferroborates $Ho_xNd_{1-x}Fe(BO_3)_4$ with temperature changing. Two compositions ($x = 1$, $x = 0.75$) demonstrate structural phase transition of the displacive type with soft lattice mode in the low-temperature phase at temperatures $T = 366$ K and $T = 203$ K consequently. The addition of Nd atoms increases interatomic spacing and, as a consequence, the temperature of structural phase transition also decreases. The increase of neodymium concentrations results in the shift into the high-frequency range of lines corresponding to oxygen vibrations in Fe–O–Fe chains which change their intensity after magnetic transitions below the Néel temperature.

The solid solutions ($x = 0.75$, 0.5, 0.25) demonstrate the emergence of the peaks corresponding to magnetoelastic interaction below Néel temperature. The ratio between integral peak intensities describes the order parameter of the magnetic phase transition. Two-magnon scattering in the spectra slightly manifests at approximately equal concentrations of holmium and neodymium atoms. When one of the atoms prevails, soft modes determined by exchange interactions in Fe–O–Fe chains are observed. The calculations confirm the data obtained in the experiment.

Acknowledgment

The reported study was funded by RFBR according to the research project 18-02-00754.

References

[1] A. A. Mukhin, G. P. Vorobev, V. Y. Ivanov, A. M. Kadomtseva, A. S. Narizhnaya, A. M. Kuzmenko, Y. F. Popov, L. N. Bezmaternikh and I. A. Gudim, Colossal magnetodielectric effect in $SmFe_3(BO_3)_4$ multiferroic, *JETP Lett.* **93**, 275 (2011).

[2] C. Ritter, A. Vorotynov, A. Pankrats, G. Petrakovskii, V. Temerov, I. Gudim and R. Szymczak, Magnetic structure in iron borates $RFe_3(BO_3)_4$ ($R = Y$, Ho): A neutron diffraction and magnetization study, *J. Phys., Condens. Matter* **20**, 365209 (2008).

[3] A. A. Demidov and D. V. Volkov, Magnetic properties of $HoFe_3(BO_3)_4$, *Phys. Solid State* **53**, 985 (2011).

[4] I. A. Gudim, E. V. Eremin and V. L. Temerov, Flux growth and spin reorientation in trigonal $Nd_{1-x}Dy_xFe_3(BO_3)_4$ single crystals, *J. Cryst. Growth* **312**, 2427 (2010).

[5] D. Jaque, Self-frequency-sum mixing in Nd doped nonlinear crystals for laser generation in the three fundamental colours: The NYAB case, *J. Alloys Compd.* **204**, 323 (2001).

[6] A. Brenier, C. Tu, Z. Zhu and B. Wu, Red–green–blue generation from a lone dual-wavelength $GdAl_3(BO_3)_4:Nd^{3+}$ laser, *Appl. Phys. Lett.* **84**, 2034 (2004).

[7] X. Chen, Z. Luo, D. Jaque, J. J. Romero, J. Garcia Sol, Y. Huang, A. Jiang and C. Tu, Comparison of optical spectra of Nd^{3+} in $NdAl_3(BO_3)_4$ (NAB), $Nd:GdAl_3(BO_3)_4$ (NGAB) and $Nd:Gd_{0.2}Y_{0.8}Al_3(BO_3)_4$ (NGYAB) crystals, *J. Phys. Condens. Matter* **13**, 1171 (2001).

[8] Y. Saeed, N. Singh and U. Schwingenschlo, First principles results on $TbAl_3(BO_3)_4$: A promising magneto-optical material, *J. Appl. Phys.* **110**, 103512 (2011).

[9] S. A. Klimin, D. Fausti, A. Meetsma, L. N. Bezmaternikh, P. H. M. Van Loosdrecht and T. T. M. Palstra, Evidence for differentiation in the iron-helicoidal chain in $GdFe_3(BO_3)_4$, *Acta Crystallogr. B Struct. Sci.* **61**, 481 (2005).

[10] A. M. Kadomtseva, Y. F. Popov, G. P. Vorobev, A. P. Pyatakov, S. S. Krotov, K. I. Kamilov, V. Yu. Ivanov, A. A. Mukhin, A. K. Zvezdin, A. M. Kuzmenko, L. N. Bezmaternykh, I. A. Gudim and V. L. Temerov, Magnetoelectric and magnetoelastic properties of rare-earth ferroborates, *Low Temp. Phys.* **36**, 511 (2010).

[11] E. P. Chukalina, M. N. Popova, L. N. Bezmaternykh and I. A. Gudim, Spectroscopic study of the magnetic ordering in $SmFe_3(BO_3)_4$, *Phys. Lett. A* **374**, 1790 (2010).

[12] E. V. Eremin, N. V. Volkov, V. L. Temerov, I. A. Gudim and A. F. Bovina, Specific features of magnetic properties of rare-earth ferroborates $Sm_{1-x}La_xFe_3(BO_3)_4$, *Phys. Solid State* **57**, 569 (2015).

[13] X.-B. Chen, T. M. Hien, K. Han, J.-Y. Nam, N. T. Huyen, S. Shin, X. Wang, S. W. Cheong, D. Lee, T. W. Noh, N. H. Sung, B. K. Cho and I.-S. Yang, Study of spin-ordering and spin-reorientation transitions in hexagonal manganites through Raman spectroscopy, *Sci. Rep.* **5**, 13366 (2015).

[14] U. Adem, L. Wang, D. Fausti, W. Schottenhamel, P. H. M. Van Loosdrecht, A. Vasiliev, L. N. Bezmaternykh, B. Buchner, C. Hess and R. Klingeler, Magnetodielectric and magnetoelastic coupling in $TbFe_3(BO_3)_4$, *Phys. Rev. B* **82**, 064406 (2010).

[15] A. De Andres, F. Agullo-Rueda, S. Taboada, C. Cascales, J. Campa, C. Ruiz-Valero and I. Rasines, Raman active phonons of $RFe_3(BO_3)_4$, R = La or Nd, single crystals, *J. Alloys Comp.* **250**, 396 (1997).

[16] A. Krylov, S. N. Sofronova, I. A. Gudim and A. N. Vtyurin, Magnetoelastic interactions in Raman spectra of $Ho_{1-x}Nd_xFe_3(BO_3)_4$ crystals, *Solid State Commun.* **174**, 26 (2013).

[17] Y. V. Gerasimova, S. N. Sofronova, I. A. Gudim, A. S. Oreshonkov, A. N. Vtyurin and A. A. Ivanenko, Infrared absorption spectra of a $Nd_{0.5}Ho_{0.5}Fe_3(BO_3)_4$ crystal, *Phys. Solid State* **58**, 55 (2016).

[18] M. N. Popova, E. P. Chukalina, T. N. Stanislavchuk, B. Z. Malkin, A. R. Zakirov, E. Antic-Fidancev, E. A. Popova, L. N. Bezmaternykh and V. L. Temerov, Optical spectra, crystal-field parameters, and magnetic susceptibility of multiferroic $NdFe_3(BO_3)_4$, *Phys. Rev. B* **75**, 224435 (2007).

[19] M. Janoschek, P. Fischer, J. Schefer, B. Roessli, V. Pomjakushin, M. Meven, V. Petricek, G. Petrakovskii and L. Bezmaternikh, Single magnetic chirality in the magnetoelectric $NdFe_3(^{11}BO_3)_4$, *Phys. Rev. B* **81**, 094429 (2010).

[20] D. Fausti, A. Nugroho, P. Loosdrecht, S. Klimin, M. Popova and L. N. Bezmaternikh, Raman scattering from phonons and magnons in $RFe_3(BO_3)_4$, *Phys. Rev. B* **74**, 024403 (2006).

[21] A. Krylov, E. Moshkina, S. Sofronova, I. Gudim, V. Temerov and A. Vtyurin, Low-temperature features of Raman spectra below magnetic transitions in multiferroic $Ho_{1-x}Nd_xFe_3(BO_3)_4$ and $Sm_{1-y}La_yFe_3(BO_3)_4$ single crystals, *Ferroelectrics* **509**, 92 (2017).

[22] E. Moshkina, A. Krylov, S. Sofronova, I. Gudim and V. Temerov, Crystal growth and Raman Spectroscopy study of $Sm_{1-x}La_xFe_3(BO_3)_4$ ferroborates, *Cryst. Growth Des.* **16**, 6915 (2016).

[23] A. S. Krylov, I. A. Gudim, I. Nemtsev, S. N. Krylova, A. V. Shabanov and A. A. Krylov, Raman study of $HoFe_3(BO_3)_4$ at simultaneously high pressure and high temperature: p–T phase diagram, *J. Raman Spectrosc.* **48**, 1406 (2017).

[24] S. N. Sofronova, Y. V. Gerasimova, A. N. Vtyurin, I. A. Gudim, N. P. Shestakov and A. A. Ivanenko, Infrared absorption spectrum of $HoFe_3(BO_3)_4$ crystal, *Vib. Spectrosc.* **72**, 20 (2014).

[25] R. P. Chaudhury, F. Yen, B. Lorenz, Y. Y. Sun, L. N. Bezmaternykh, V. L. Temerov and C. W. Chu, Magnetoelectric effect and spontaneous polarization in $HoFe_3(BO_3)_4$ and $Ho_{0.5}Nd_{0.5}Fe_3(BO_3)_4$, *Phys. Rev. B* **80**, 104424 (2009).

[26] N. Tristan, R. Klingeler, C. Hess, B. Buchner, E. Popova, I. A. Gudim and L. N. Bezmaternykh, Thermodynamic properties of $NdFe_3(BO_3)_4$, *J. Magn. Magn. Mater.* **316**, e621 (2007).

[27] A. Krylov, E. M. Kolesnikova, L. I. Isaenko, S. N. Krylova and A. N. Vtyurin, Measurement of Raman-scattering spectra of $Rb_2KMoO_3F_3$ crystal: Evidence for controllable disorder in the lattice structure, *Cryst. Growth Des.* **14**, 923 (2014).

[28] J. A. Campa, C. Cascales, E. Gutierrez-Puebla, M. A. Monge, I. Rasines and C. Ruiz-Valero, Crystal structure, magnetic order, and vibrational behavior in iron rare-earth borates, *Chem. Mater.* **9**, 237 (1997).

[29] D. L. Rousseau, R. P. Bauman and S. P. S. Porto, Normal mode determination in crystals, *J. Raman Spectrosc.* **10**, 253 (1981).

[30] M. B. Smirnov and V. Y. Kazimirov, LADY: Software for lattice dynamics simulations, *JINR Commun.* E14-2001-159 (2001).

[31] P. Ewald, Die berechnung optischer und elektrostatischer gitterpotentiale, *Ann. Phys.* **369**, 253 (1921).

[32] F. Herman, Lattice vibrational spectrum of germanium, *J. Phys. Chem. Solids* **8**, 405 (1959).